Computers & Structures Vol. 30, No. 5, pp. 1147-1151, 1988
Printed in Great Britain.

0045-7949/88 $3.00 + 0.00

FINITE ELEMENT INVESTIGATION OF PLANE STRAIN ASYMMETRIC FULLY PLASTIC FRACTURE

G. A. Kardomateas†
Massachusetts Institute of Technology, Cambridge, MA 02139, U.S.A.

(*Received* 24 *November* 1987)

Abstract—Crack initiation and early growth in asymmetric fully plastic plane strain configurations in power-law hardening materials is investigated numerically via the finite element method. In such asymmetric configurations a single shear band is present instead of the two shear bands of the symmetric case. Results for two strain hardening exponents, $n = 0.12$ and $n = 0.24$, indicate that cracking occurs at an angle of 39–43° from the transverse, smaller than 45° due to the higher triaxiality. The direction of cracking is closer to 45° for lower strain hardening exponents and is within 2° of experimental values. The stress and strain field is consistent with the singular power-law, extended for Mixed Modes I and II, HRR fields. The far-field displacement vector is not along the shear band but at about 68–70° from the transverse at initiation, indicating the presence of a Mode I component. Early growth, studied by successive removal of elements reaching unit damage, results in a crack growth per unit displacement for the lower hardening case of about twice that of the higher hardening one.

INTRODUCTION

Asymmetric plane strain specimens have been used [1] to study crack growth along a single shear band. Such cases may occur when a weld fillet or a harder heat-affected zone on one side of the crack suppresses the other shear zone that would appear in a symmetric specimen. Based on Shih's extension to mixed mode [2] of the HRR fields [3, 4], McClintock and Slocum [5] developed an approximate formulation for the accumulation of damage directly ahead of an asymmetric crack. The crack was assumed to follow the center of a 45° shear band and the far-field displacement was assumed to be parallel to the shear band. It was found that the initiation displacement was of the order of the fracture process zone size ρ. This solution, which is based on pure Mode II deformation and a superposition of stationary singularities, gave practically no change in crack growth rate with decreasing strain hardening exponent. However, tests have shown that the far field displacement vector is not at 45° but is more axial, at an angle of about 60° from the transverse. In addition, a lower strain hardening exponent n was found to strongly increase the crack growth rate. In the problem under consideration, the nonhardening field consists of a single slip line at 45° from the transverse. Strain hardening, however, causes the deformation field to fan out. The effect of the finite width of the shear band can be captured with a finite element investigation. In the following, the finite element method is used to study crack initiation and early growth in fully plastic plane strain asymmetric specimens.

† Present address: General Motors Research Laboratories, Engineering Mechanics Department, Warren, MI 48090-9055, U.S.A.

TECHNIQUE

The finite element grid used is indicated in Fig. 1, with the details of the refined mesh for the first circle around the crack tip shown in Fig. 2. An increased element concentration near the 45° line is used to account for the high strain gradients there. Angular spacings of 3.75° for four sectors, 7.5° for two sectors, 15° for four sectors and 30° for nine sectors are used. Minimum radial size for the 3.75° elements is $\rho = 0.01$ mm, the approximate value for the mean inclusion spacing size. The radial size ratio was $s = 1.155$ for the 3.75° sectors becoming s^2 for the 7.5° sectors, s^4 for the 15° sectors, and s^8 for the 30° sectors. The net ligament of the specimen is $l_0 = 2.55$ mm. Eight-node plane strain isoparametric

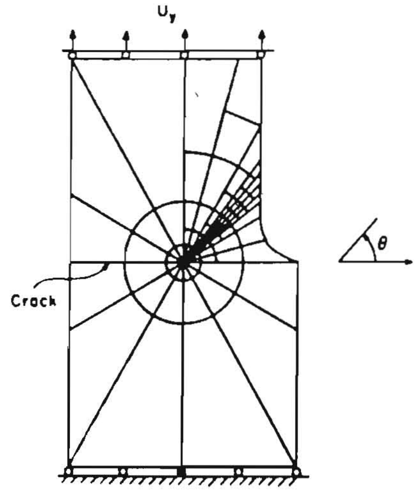

Fig. 1. The finite element mesh.

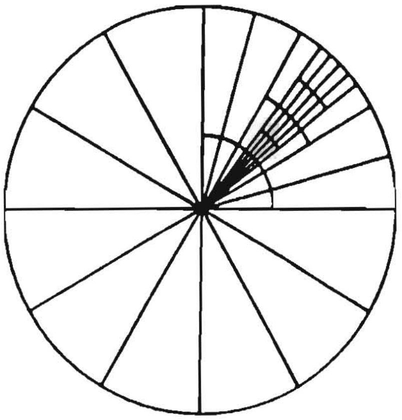

Fig. 2. Detail of the finite element mesh around the crack tip.

elements are used. The mesh consisted of a total of 207 elements with 722 nodes and 1444 degrees of freedom. The nodes at the bottom were on rollers with the center node pinned. An axial displacement with zero shear traction was applied at the nodes of the upper end. The analysis was carried on a Data General computer and the general purpose finite element code ABAQUS [6] was used.

The mesh was checked by laying out the theoretical strain distribution for the elastic and low hardening $n = 1/13$ HRR [3, 4] field and comparing with the assumed (from the chosen 8-node element type) linear variation of strains within the element. The radial variation in strain for the elastic solution showed a maximum deviation of 15% for the first element around the tip. For the HRR $n = 1/13$ solution the deviation was 33%, dropping to 5.6% for the second element. The angular distribution in $\epsilon_{r\theta}$ showed a maximum deviation of 8% from the HRR for the 30° sectors. In addition, a circular portion of the finite element mesh consisting of 16 radially elements at the finest sectors was tested by imposing Mode I HRR displacement boundary conditions. The HRR singularity in $\epsilon_{r\theta}$ was reproduced with no more than 5% deviation in all elements except the first one, where the maximum deviation was 14% at the first integration point.

The material is modeled as isotropic power-law hardening: the stress σ is given in terms of the plastic strain ϵ^p, the flow stress at unit strain σ_1, a strain hardening exponent n, and a pre-strain ϵ_0 by

$$\sigma = \sigma_1 (\epsilon_0 + \epsilon^p)^n. \tag{1}$$

Two cases were considered, $n = 0.24$, $\sigma_1 = 826$ MN m^2, yield strength $Y = 333$ MN/m^2 and $n = 0.12$, $\sigma_1 = 909$ MN/m^2, $Y = 435$ MN/m^2.

The fracture criterion of McClintock *et al.* [7] is used, by which it is postulated that fracture due to micro-void coalescence occurs when a quantity η, named damage, reaches a critical value of unity. The damage is expressed in terms of a hole growth ratio F_l, the principal shear strain γ, and the triaxiality, defined as the ratio of the mean normal stress σ to principal shear strain τ. In terms of the equivalent stress and strain

$$\tau = \sigma_{eq}/\sqrt{3}, \quad \gamma = \epsilon_{eq}/\sqrt{3}, \tag{2}$$

the damage is expressed as

$$\eta = \frac{1}{\ln F_l}\left[\ln\sqrt{(1+\gamma^2)} + \frac{\gamma}{2(1-n)}\sinh\left(\frac{(1-n)\sigma}{\tau}\right)\right]. \tag{3}$$

The critical displacement for growth initiation occurs when the damage becomes unity at a point (ρ, θ_c) where ρ is the fracture process zone size and θ_c is the critical orientation. To study the first steps of crack growth, the element removal technique was used. The crack was grown by removing elements as they reached a damage of unity.

RESULTS AND DISCUSSION

The axial displacement, U_y, at the upper end was gradually increased and the damage from (3) was calculated at each site around the tip. Cracking occurs when the fracture criterion of $\eta = 1$ is first satisfied.

The initiation conditions (critical orientation from the transverse, θ_c, critical strain γ_c, critical triaxiality σ/τ, far-field displacement u_i/ρ) are shown in Table 1. The crack tip initiation displacement is of the order of the mean inclusion spacing size as was also found in [5]. A critical orientation of 39–43° from the transverse and a far-field displacement vector orientation of about 68–70° at initiation can be compared with the values of 38–41° for the crack direction and 58–69° for the displacement vector at initiation from tests [1]. The lower hardening $n = 0.12$ case results in fracture closer to the shear band, as found experimentally [1].

To describe the Model I component, a mixity parameter M^p was introduced by Shih [2], defined in terms of the near field stresses by

$$M^p = \frac{2}{\pi}\tan^{-1}\left|\lim_{r\to 0}\frac{\sigma_{\theta\theta}(r, \theta = 0)}{\sigma_{r\theta}(r, \theta = 0)}\right|. \tag{4}$$

The mixity parameter varied from 0 for pure Mode II to 1 for pure Mode I. This parameter can be evaluated by using either the initial crack direction $\theta = 0°$ or the final (critical) one $\theta = \theta_c$, giving values as shown in Table 1. Notice that the above definition of the Mode I mixity is with respect to shearing and crack advance at $\theta = 0$ for both the limiting cases $M^p = 0$ or 1. In the problem at hand, pure Mode I is crack advance along the line $\theta = 0$ (corresponding to the symmetric case) and pure Mode II would be relative deformation and crack advance along the 45°

Table 1. Results of the finite element study

		$n = 0.12$	$n = 0.24$
Initiation conditions			
Critical angle from transverse	θ_c	43.1°	39.4°
Far-field displacement components	U_y/ρ U_x/ρ	2.1 0.782	1.8 0.737
Displacement vector angle from transverse	ϕ	69.5°	67.7°
Displacements at crack tip	$u_x(x = 0, y = 0)/\rho$ $u_y(x = 0, y = 0)/\rho$	0.134 0.518	0.192 0.564
Principal shear strain	γ_c	0.246	0.327
Triaxiality	σ/τ	2.18	1.995
Mixity parameter:			
Mode I mixity, as defined by Shih [2] (based on stresses)	M^p (rel. to $\theta = 0°$) (rel. to $\theta = \theta_c$)	 0.936 0.717	 0.927 0.710
Displacement based Mode I mixity	M_I^*	0.752	0.815
Early growth			
Far field displacement, per projected crack advance (four steps, 1.9% of the ligament)	$\Delta u/\Delta l$	0.075	0.143

shear band (nonhardening limit). Alternatively, for experiments and finite element studies, a definition of a Mode I mixity in terms of the displacement field is helpful

$$M_I^* = \frac{2}{\pi}\tan^{-1}\left|\lim_{r\to 0}\frac{u_\theta(r,\pi) - u_\theta(r,-\pi)}{u_r(r,\pi) - u_r(r,-\pi)}\right|. \quad (5)$$

Values for this parameter are also shown in Table 1. Notice that for the non-hardening rigid plastic pure Mode II limit with a single slip line at $\theta = 45°$, $M_I^* = 0.5$ for the crack at $\theta = 0°$ but $M_I^* = 0$ for the crack at $\theta = 45°$.

Figure 3a shows the angular variation of the $\sigma_{r\theta}$ stress component. The curve is consistent with Shih's [2] curves and has a maximum near $\theta = 65°$. This compares with the case $M^p = 1, n = 1/13$ with a maximum near 88°, whereas the case of $M^p = 0$ has a maximum $\sigma_{r\theta}$ at $\theta = 0$. Furthermore, the maximum for $n = 1/13$, $M^p = 0.82$ is near 55° and for $n = 1/13$, $M^p = 0.79$ is near 40° [2]. The θ-variation of $\epsilon_{r\theta}$ is shown in Figs 3b and 3c. Of the two peaks in $\epsilon_{r\theta}$, the one for positive θ is the dominant one, the other peak tending to vanish during growth when the Mode I component is reduced [2].

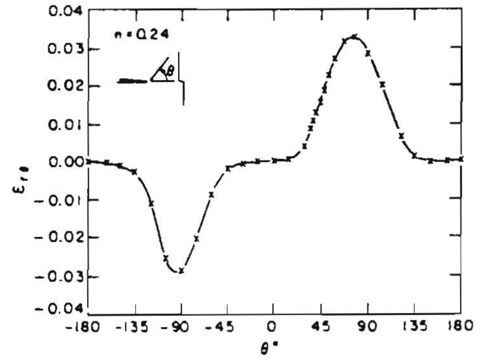

Fig. 3b. Angular variation of the shear strain $\epsilon_{r\theta}$ at initiation (at $r = 5\%$ of the ligament) for $n = 0.24$.

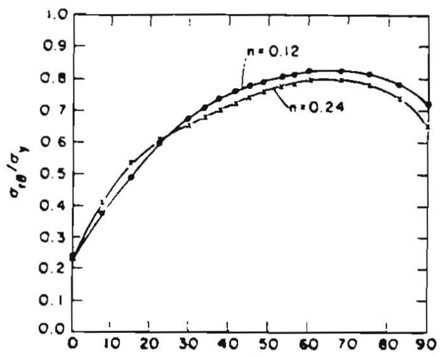

Fig. 3a. Angular variation of the shear stress $\sigma_{r\theta}$ at initiation (at $r = 5\%$ of the ligament).

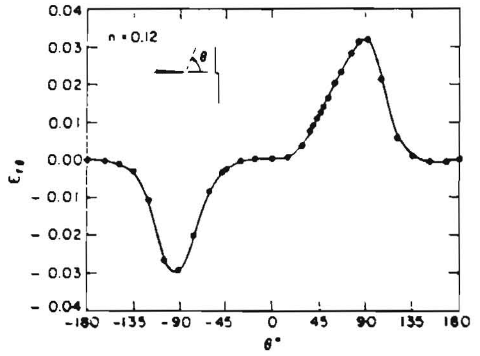

Fig. 3c. Angular variation of the shear strain $\epsilon_{r\theta}$ at initiation (at $r = 5\%$ of the ligament) for $n = 0.12$.

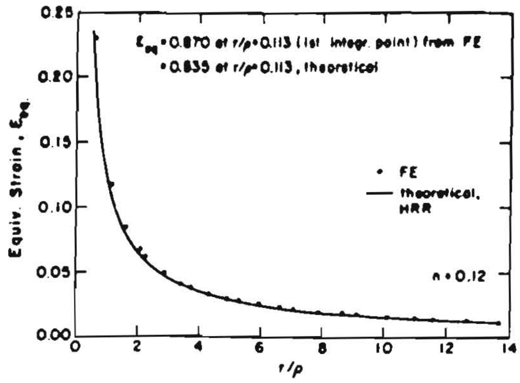

Fig. 4. Radial variation of the equivalent plastic strain vs the one for the HRR singularity at the critical angle.

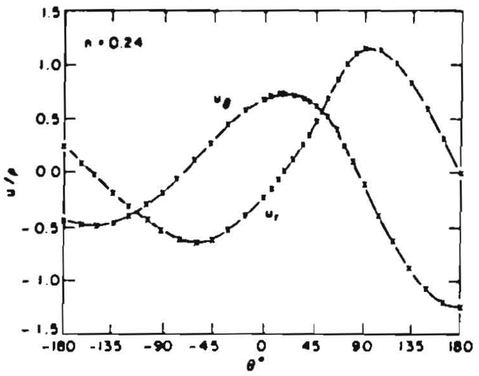

Fig. 6a. Angular variation of the near tip displacement field (at r = 5% of the ligament) for $n = 0.24$.

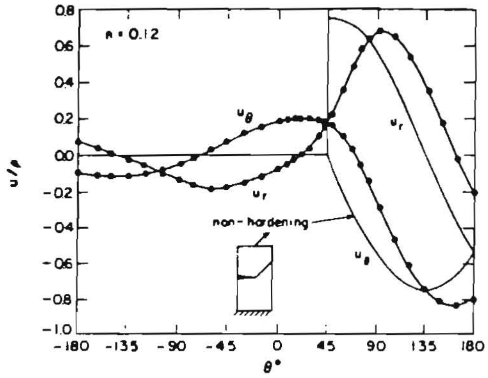

Fig. 6b. Angular variation of the near tip displacement field (at r = 5% of the ligament) for $n = 0.12$. The variation of the displacements for the nonhardening limit is also illustrated.

The radial variation of the equivalent strain along the critical orientation is of interest. The asymptotic solution for power-law hardening materials yield singularities in the stress and strain, respectively, of the forms $r^{-n/(n+1)}$ and $r^{-1/(n+1)}$. A comparison between such a theoretical variation and the finite element results for the case $n = 0.12$ is shown in Fig. 4.

Figure 5 shows the axial displacement of the upper flank relative to the lower flank at the initiation point. The components of the relative displacement of the crack tip $u_x(x=0, y=0)$ and $u_y(x=0, y=0)$ are included in Table 1. A higher CTOD occurs in the higher hardening case. Figures 6a and 6b show the angular variation of the near tip displacement field for the two hardening exponents $n = 0.24$ and $n = 0.12$, along with the non-hardening limit. The latter one, which is the case of pure shear at 45°, is simply

$$
\begin{aligned}
&u_r = u_\theta = 0 \quad \text{for } \theta < 45^\circ \\
&u_r = U\cos(\theta - 45^\circ) \\
&u_\theta = -U\sin(\theta - 45^\circ) \quad \text{for } \theta \geq 45^\circ,
\end{aligned} \tag{6}
$$

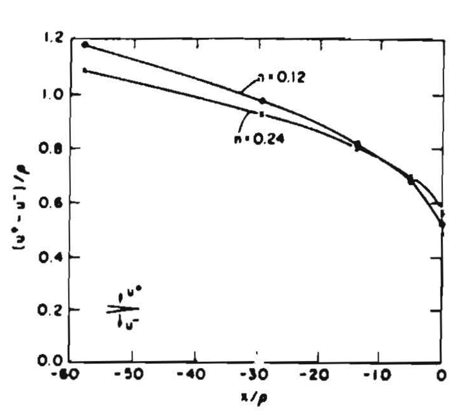

Fig. 5. Displacement of the upper crack flank relative to the lower flank.

where $U = U_x \cos 45^\circ$ is the applied far-field displacement along the slip line.

The far-field displacement (displacement at the upper boundary) components U_x and U_y at the initiation point are also included in Table 1, together with the far-field displacement vector orientation from the transverse, ϕ. The value of ϕ = 68–70°, instead of 45°, indicates that we cannot consider the far-field displacement taking place parallel to the shear band, as assumed by McClintock and Slocum [5]. We can observe that the displacement vector at initiation is more axial for the lower hardening case with larger M^p. The higher triaxiality for angles smaller than 45° is the main reason for the cracking direction deviating towards the transverse. The triaxiality is smaller for $n = 0.24$ because of the smaller Mode I mixity M^p.

Tests have shown that, in the asymmetric case, the lower hardening alloys exhibit a maximum crack growth rate more than twice that of the higher hardening alloys [1]. The finite element mesh of Fig. 1 was used to study the early growth. The crack was grown by successive removal of the most heavily damaged element. After initiation and removal of the most damaged element, the far-field displacement is further increased until critical damage $\eta = 1$ occurs in the next row of elements. At this point the next step of crack growth takes place by removing the critical element. After growth by four steps (1.9% of the ligament) it is found that the average displacement per unit projected crack advance $\Delta u/\Delta l$ is about 88% smaller for the lower hardening $n = 0.12$ case than for the higher hardening $n = 0.24$ case (Table 1). Another noteworthy result is that the far-field displacement vector U becomes less axial as the crack grows. For the case $n = 0.12$, at the end of the fourth step, the angle of the displacement vector from the transverse is $\phi = 67.6°$ instead of the initiation value of $\phi = 69.5°$. Decreasing ϕ angles with crack growth have been experimentally observed. During these steps the critical elements are at the same angular sector and no appreciable acceleration of the crack is observed.

CONCLUSIONS

A finite element investigation of fully plastic asymmetric specimens with a single slip band, which would simulate, for example, defects near a weld, has provided the stress, strain and displacement fields around the tip. Results indicate the presence of a large Mode I component with the far-field displacement vector at initiation not along the 45° shear band but at an angle of about 68° from the transverse. The initiation conditions are found by using the fracture criterion for hole growth in terms of the triaxial stress and the principal shear strain. The critical direction is at 39–43°, less than 45° from the transverse, increasing for a lower strain hardening exponent. Displacement to crack initiation is about twice the fracture process zone size. Stress and strain fields are consistent with the solutions for the Mixed Mode extended HRR fields. Early growth, studied by successive removal of the most damaged element, results in a crack growth rate for the lower hardening case of about twice that of the higher hardening one while the angle of the far-field displacement vector from the transverse is found to decrease with crack growth.

Acknowledgements—The financial support of the Office of Naval Research, Contract N0014-82K-0025, and the interest and encouragement of the Project Monitor, Dr Y. Rajapakse, are both gratefully acknowledged.

REFERENCES

1. G. A. Kardomateas and F. A. McClintock, Tests and interpretation of mixed mode I and II fully plastic fracture from simulated weld defects. *Int. J. Fracture* **35**, 103–124 (1987). See also G. A. Kardomateas, Mixed mode I and II fully plastic crack growth for simulated weld defects. Ph.D. thesis, Department of Mechanical Engineering, Massachusetts Institute of Technology, Cambridge, MA (1985).
2. C. F. Shih, Small scale yielding analysis of mixed mode plane strain crack problems. *Fract. Anal.* ASTM STP **560**, 187–210 (1974).
3. J. W. Hutchinson, Singular behavior at the end of a tensile crack in a hardening material. *J. Mech. Phys. Solids* **16**, 13–31 (1968).
4. J. R. Rice and G. F. Rosengren, Plane strain deformation near a crack tip in a power law hardening material. *J. Mech. Phys. Solids* **16**, 1–12 (1968).
5. F. A. McClintock and A. H. Slocum, Predicting fully plastic mode II crack growth from an asymmetric defect. *Int. J. Fracture* **27**, 49–62 (1985).
6. ABAQUS, Habbit, Karlsson and Sorensen, Inc., Providence, RI
7. F. A. McClintock, S. M. Kaplan and C. A. Berg, Ductile fracture by hole growth in shear bands. *Int. J. Fracture Mech.* **2**, 614–627 (1966).